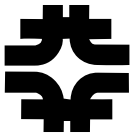

Fermilab

Doc Number: Beams-doc-2388
Version: 1.0
Type: Note

Thermal Calculation for MI8 Collimators

Alex Chen, Mechanical Support Department
Bruce C. Brown, Main Injector Department
Accelerator Division
Zhijing Tang, Mechanical Department
Particle Physics Division
*Fermi National Accelerator Laboratory**
P.O. Box 500
Batavia, Illinois 60510
10 August 2006

*Operated by the Universities Research Association under contract with the U.S. Department of Energy

Thermal Calculations for MI8 Collimators

Abstract

A collimation system for the Fermilab Booster to Main Injector transfer line (MI8 line) has been designed and installed. This system will remove particles in the beam halo from 8 GeV Booster beam before it arrives at the Main Injector. A pair of 5 ton collimators, with horizontal and vertical motion, is installed between the gradient magnets in half-cell 836 and an identical system is placed one cell away (about 90^o in phase advance) at 838. The static and dynamic thermal response of this system to energy deposited by 8 GeV protons has been calculated to examine peak temperatures and temperatures at thermocouple locations. Results of these calculations will be used to establish temperature limits for device protection. We will explore the possibility of monitoring the integrated beam power lost to the collimators by measurement of the temperature rise integrated over the time of operation.

Introduction

In order to provide a more precisely tailored beam as input to the Main Injector, a set of collimators has been installed in the Booster to Main Injector transfer line. Following the design goals for the Booster Collimators [1], we assume a Booster output intensity of $5x10^{12}$ protons per pulse and operation at 10 Hz or a beam power of 64k Watts. If a part per thousand of the beam were symmetrically scraped, we believe that it would reduce the number of Main Injector locations with significant residual radiation. However, if the beam position is not stable, the scraping will become asymmetric and a larger beam fraction will be scraped in each collimator pair. The radiation simulation indicates that the primary limitation on the collimator use will come from production of radioisotopes in the materials outside but adjacent to the tunnel walls where it can be leached into water to be pumped to the surface by the sump pump systems. This will limit the beam power which can be safely scraped to about 1% of 64k Watts. Within this framework, we wish to understand the thermal properties of the collimators so that beam can be inhibited when collimator temperatures indicate that the desired scraping rate has been exceeded. Note that additional loss information from loss monitors will provide redundant loss limits for machine component protection. In addition, the temperature rise in the collimator is related to the beam power deposited. We will examine the temperature response in the expectation that a useful measure of the beam power of the collimated beam can be obtained from a time integral of the temperature rise.

The MI8 collimation system consists of a vacuum liner as primary absorber surrounded by an iron absorber and a marble shield as described in Reference [2]. The design concept assumes that beam will be scraped in a corner so that, for example, the left side and the bottom of the beam will be scraped with one collimator while the next collimator in the same lattice cell will scrape the right side and top. A simulation of absorption of the beam in a corner of the collimator was carried out using MARS [3]. In addition to other results of interest for radiation protection, a 3-dimensional energy deposition map was created. Using this as input, calculations of the equilibrium and dynamic thermal response has been carried out using ANSYS [4][5].

Collimator Design, Overview

The collimator is comprised of the vacuum liner (item 3) surrounded with steel absorber (item 4) and marble (item 5). Figure 1 shows the collimator with its motion system.

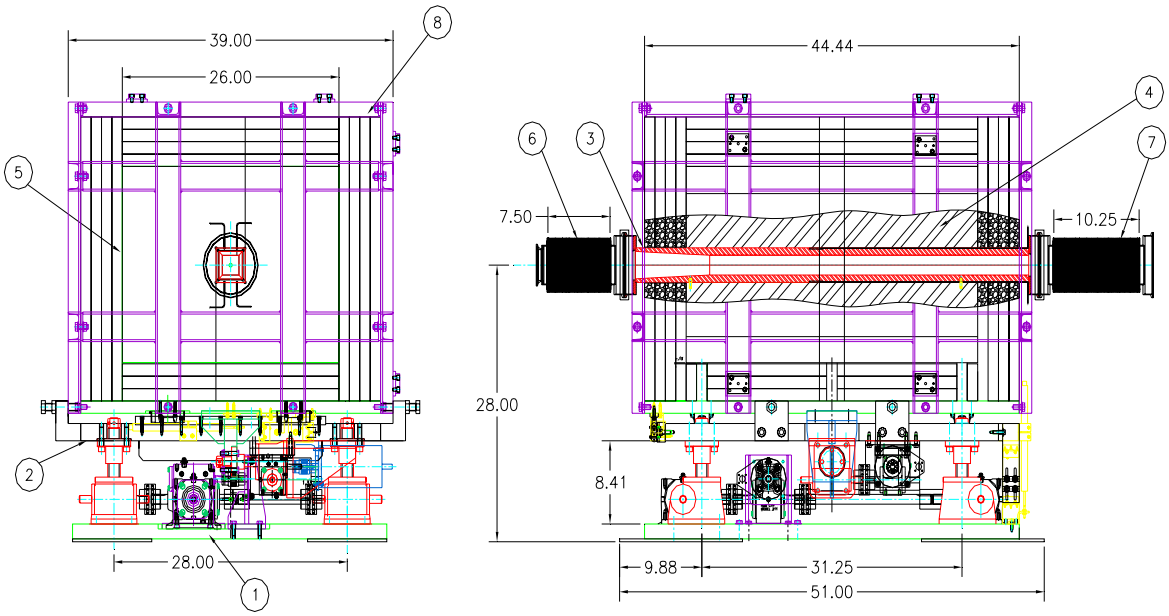

Figure 1 Collimator Assembly

1- Base Plate Assembly; 2 - Support Plate Assembly; 3 - Vacuum Liner Weldment; 4 - Steel Shielding Block Assembly; 5 - Marble plates; 6 - 7.5" Bellows Weldment; 7 - 10.25" Bellows Weldment; 8 – Aluminum Frame.

Vacuum Liner

The vacuum liner (Figure 2) serves as the primary absorber. It is designed to provide an impact point for the intercepted beam with low outscattering. The stainless steel blocks create a device with a 2" square vacuum aperture and a 3.5" square outer surface which is 47" long. A tapered portion is provided at the upstream end to increase the penetration of intercepted particles. This chamfer is 8.94" long with a taper of 2.56°. Since we expect the beam which strikes the collimator to be most intense at the downstream end of this chamfer, the radiation simulation will employ a beam whose core is near a corner of the liner with lost particles striking the chamfer. The wall thickness of 0.75" in the body is only 0.35" at the upstream end. Particles parallel to the collimator axis will strike the chamfer at 45 milliradian angle.

Two grooves of 0.125" width are cut in the top and bottom of the absorber block at 0.75" left and right of the centerline for mounting thermocouples. These grooves extend from the downstream end to within 19.84" of the upstream end which places them 10.9" downstream of the end of the tapered portion. Four J Type thermocouples (OMEGA part #: XCIB- J -4 -3 -10) are glued into the vacuum liner thermocouple slots. For each collimator, we will instrument two channels of thermocouple readout with the other two devices available as spares. The thermocouple junctions are located ~11" down stream from a collision point. An additional thermocouple (OMEGA part #: 5TC-GG-J -24-36) is installed for each collimator. It is initially mounted on the wall side of the vacuum liner upstream of the marble which places it nearer the thermal hot spot. Following thermal studies, one or more of these thermocouples may be mounted on an upstream magnet to monitor tunnel temperature.

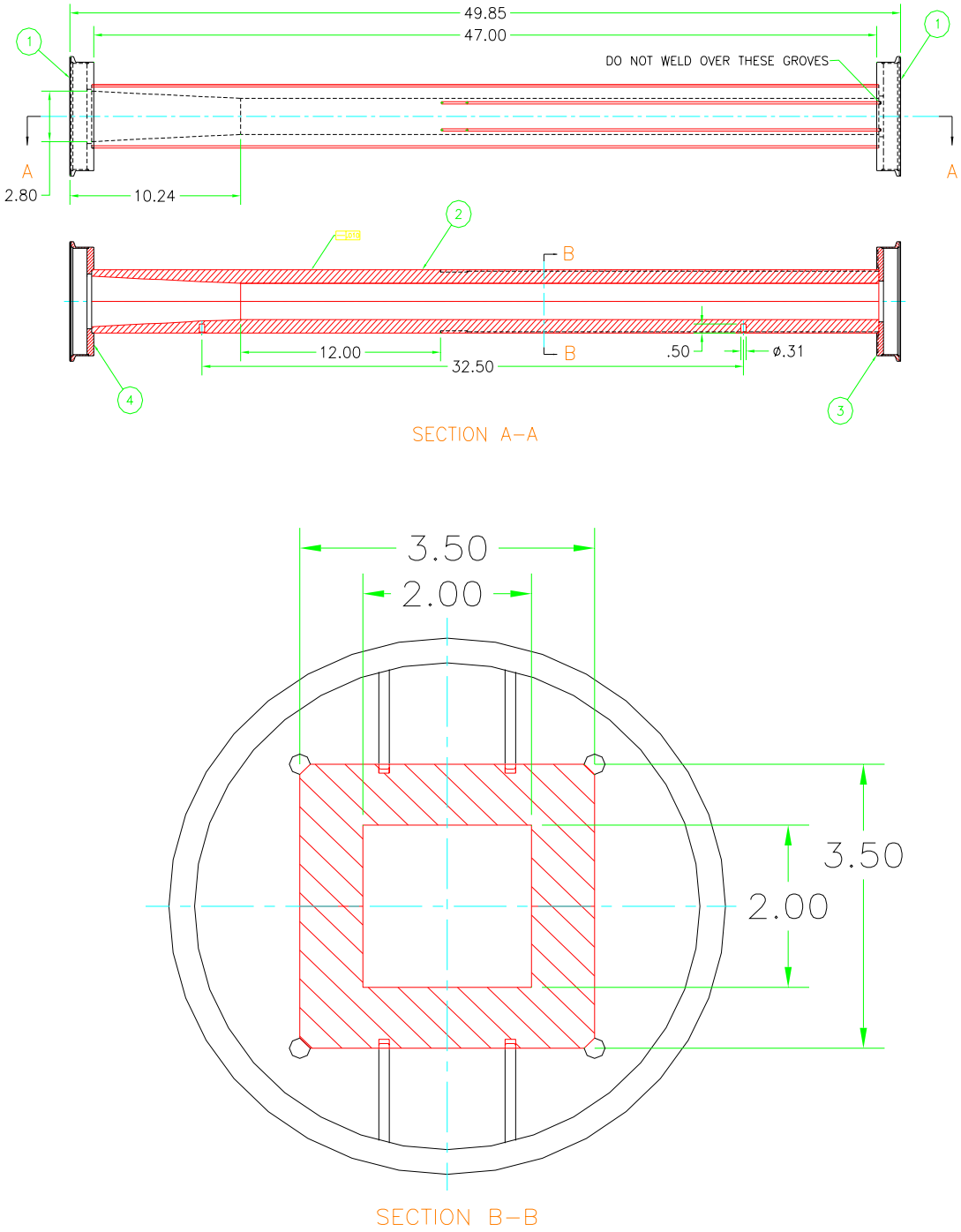

Figure 2 Stainless Steel Vacuum Liner

1- 6" Booster QD Flange; 2 – Tapered Block; 3 – End Plate DS; 4 – End Plate – US.

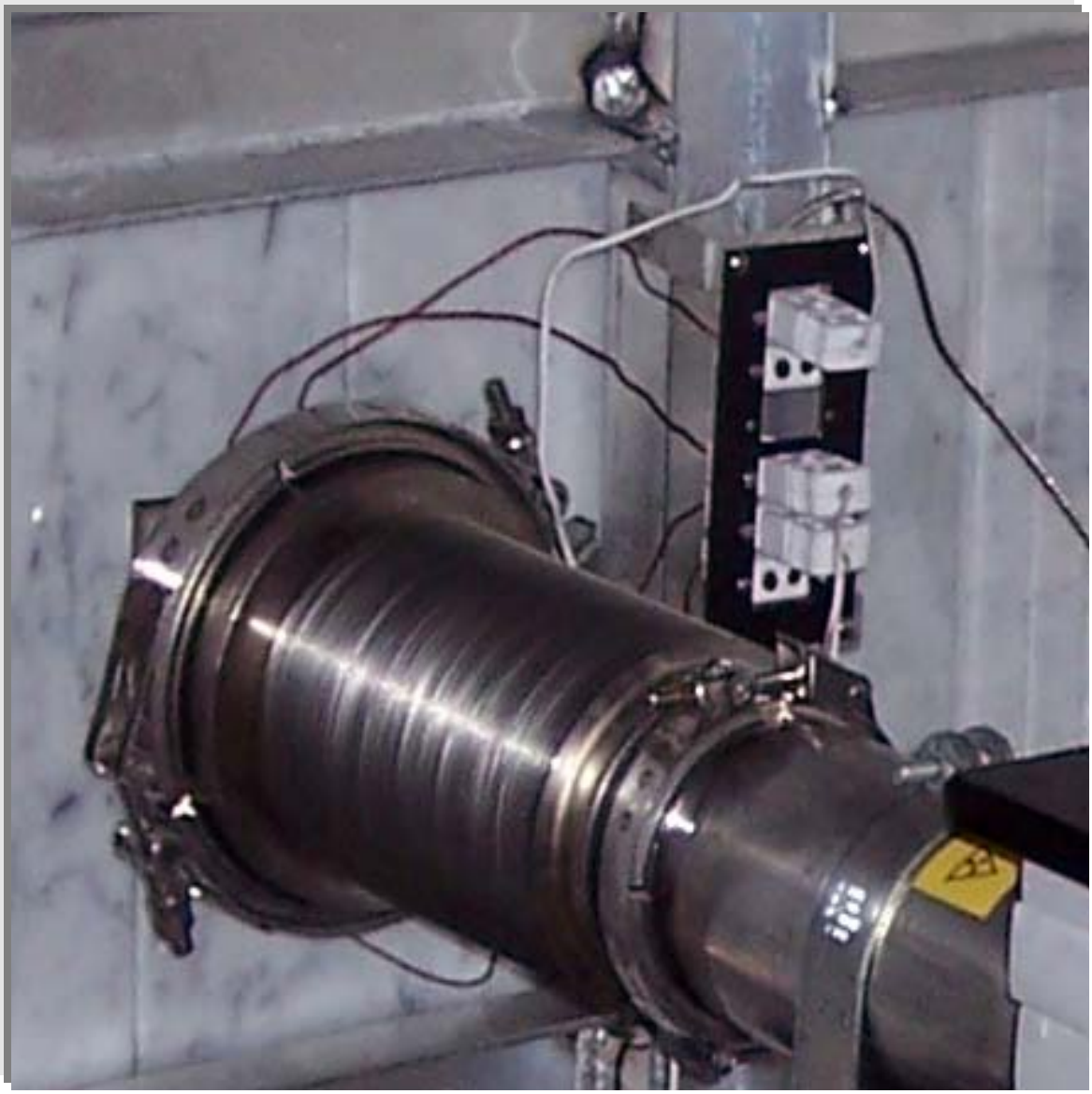

Figure 3 Thermocouple connectors panel.

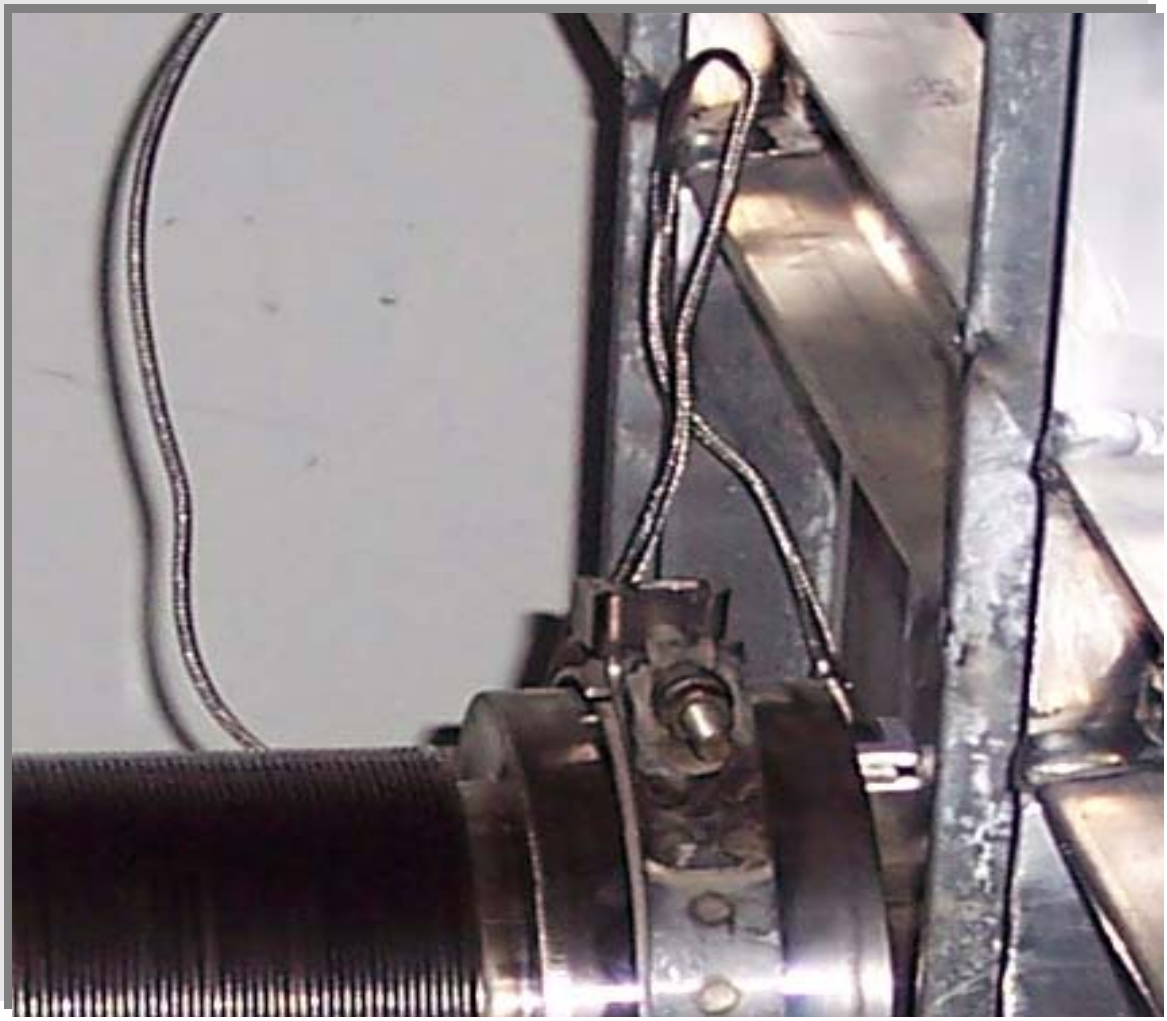

Figure 4 Upstream vacuum liner thermocouple.

Energy Deposition Calculation and Model for ANSYS

The beam energy deposit has been calculated assuming a beam whose core passes near a corner of the 2"x 2" aperture of the vacuum liner. Nominal beam size parameters have been used but we believe that details of the beam will not impact the conclusions of this study. Halo protons will strike the collimator with most of them impacting near the end of the chamfer.

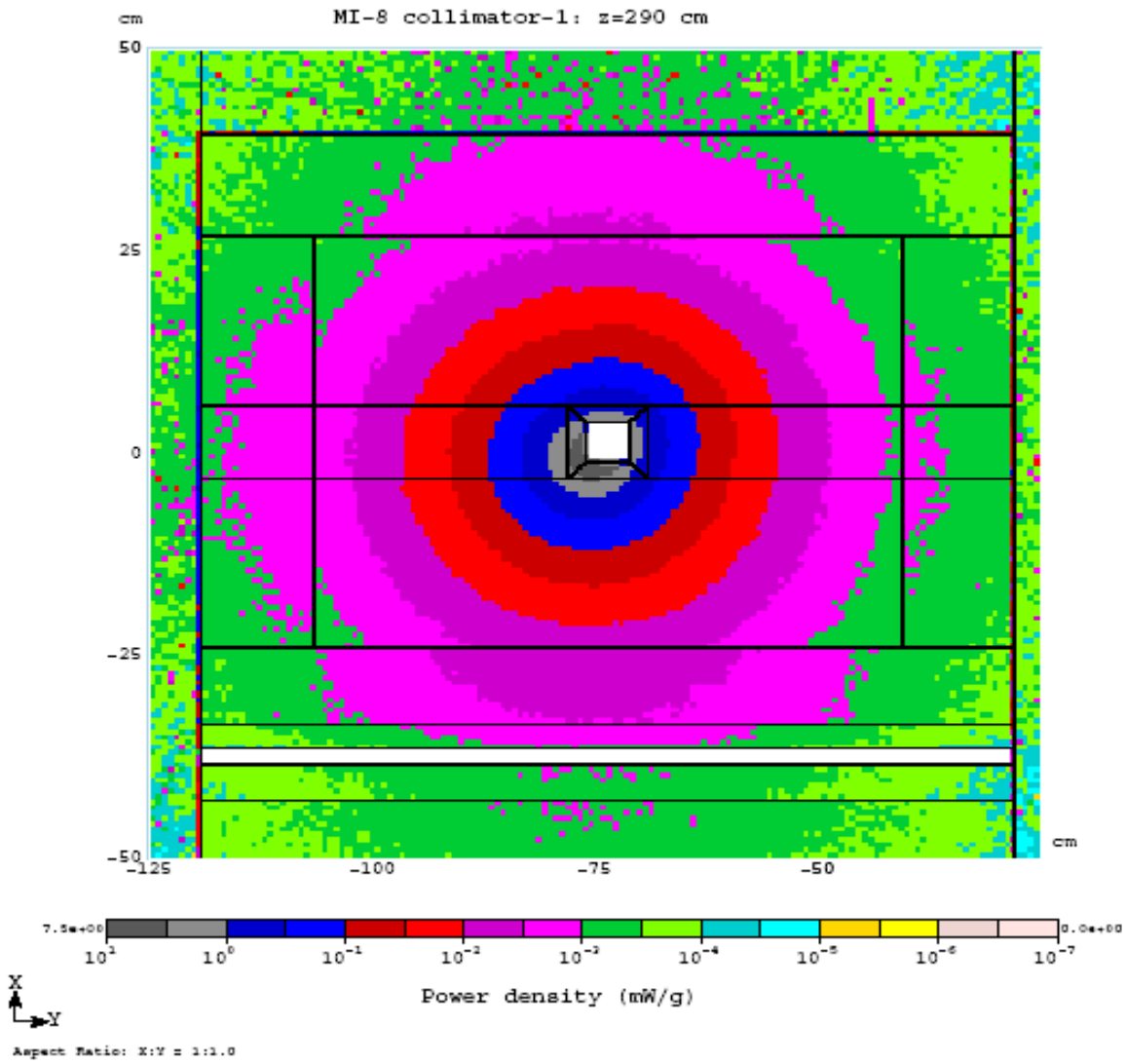

Figure 5 MARS results: Cross-sectional Distribution of Power Density

Fig 5 and Fig 6 show the power density distribution in 2D, from MARS simulation by Nikolai Mokhov [3]. Collimated protons deposit energy in a shower of secondary particles. Ionization from the protons and their secondary particles deposits energy in the collimator as they pass through. This energy heats the steel. In Fig 5, the power density is shown in cross section at the shower maximum in the first collimator (z=290 cm in coordinates of the MARS simulation, see figure 3). We see that the contours of power density are centered at the low-left corner of the vacuum tube and are axially symmetric. Figure 6 shows the longitudinal distribution for a 5 cm vertical slice (from -80 cm to -75 cm) centered on the beam axis. The collimator pair is shown with design transverse positioning to provide beam interaction in each collimator. The maximum energy deposition in each collimator occurs at the end of tapered portion (or the start of straight portion).

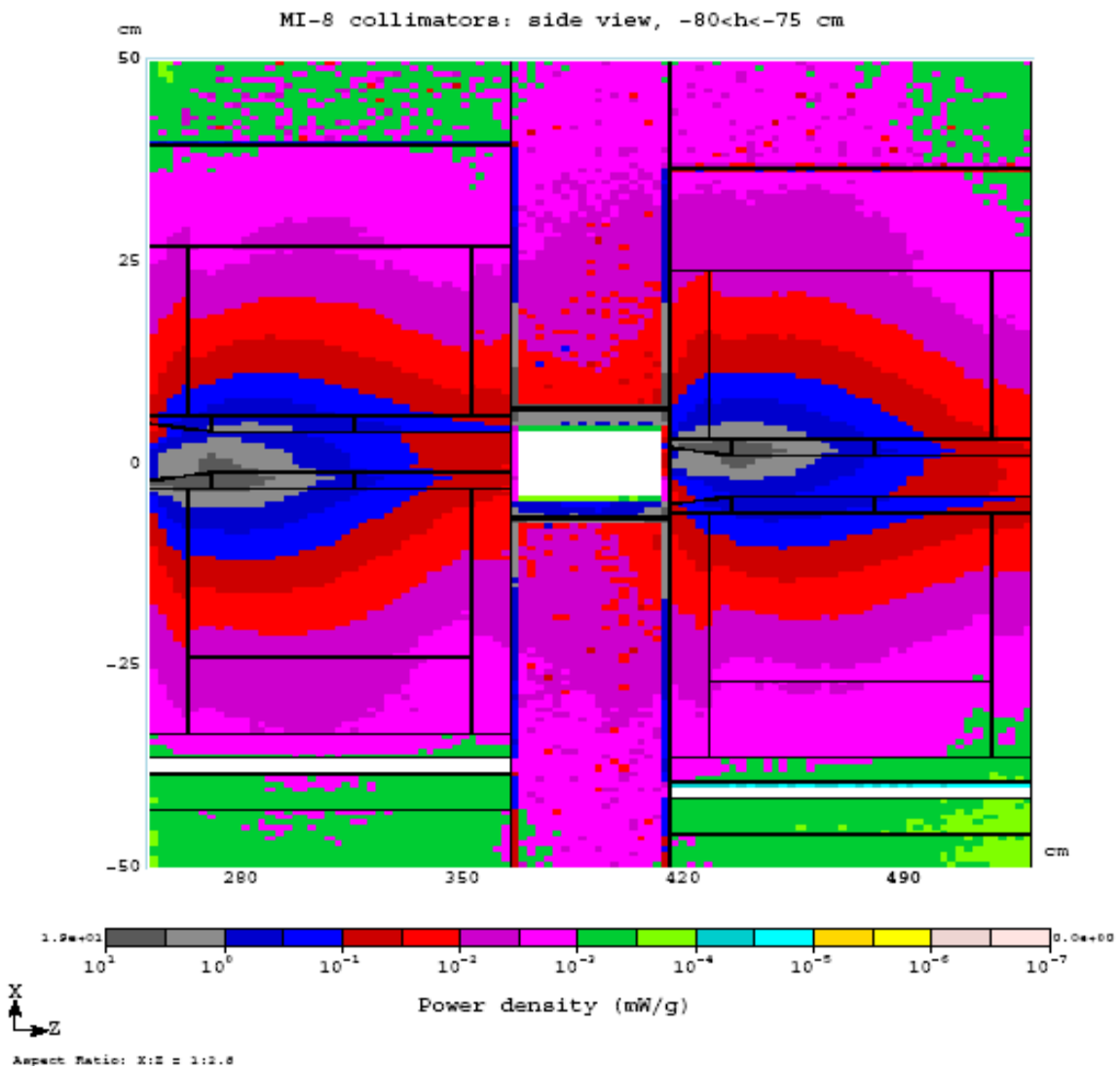

Fig. 6 MARS results: Lateral and Longitudinal distribution of Power Density in collimator pair. Beam passes near lower left corner of upstream collimator and upper right corner of downstream collimator.

Because the thermal calculation will be carried out in 3D, and modeling in ANSYS is different from MARS modeling, the power density data cannot be used directly in ANSYS. It is necessary to construct a formula which can closely represent the data from MARS. To match the 2D plots and general characteristics of power density distribution, the formula was designed as:

$$P(t,r,z) = F(t)Er(r)El(z)$$

Where

$$E_r = \exp\left(-1.9688\times10^{-4}\, r^3 + 0.013688\, r^2 - 0.49974\, r + 2.0964\right),$$

$$E_l = \exp\left(6.5868\times10^{-6}\, z^3 - 8.8754\times10^{-4}\, z^2 - 0.025163\, z + 1.933\right).$$

with r the radial distance from the lower left corner of the vacuum liner, near the beam center and z the absolute value of the distance from the longitudinal peak of the energy deposition. The parameters of this formula were determined by best fitting as shown in Fig. 7 and Fig 8. The data sets were sampled from 2D MARS plots.

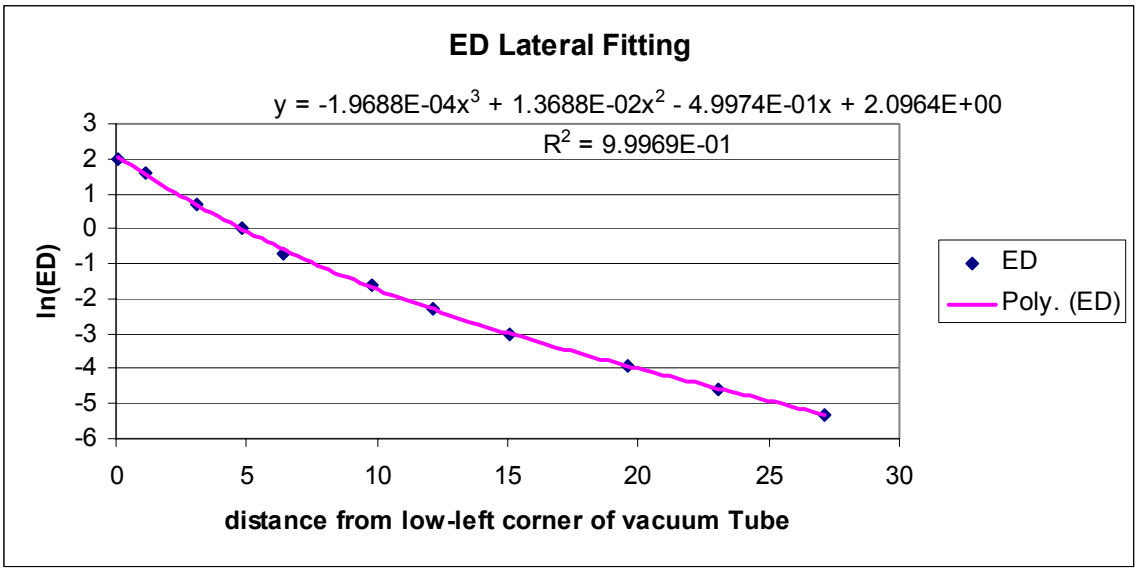

Fig 7 Fitting Radial formula $E_r(r)$

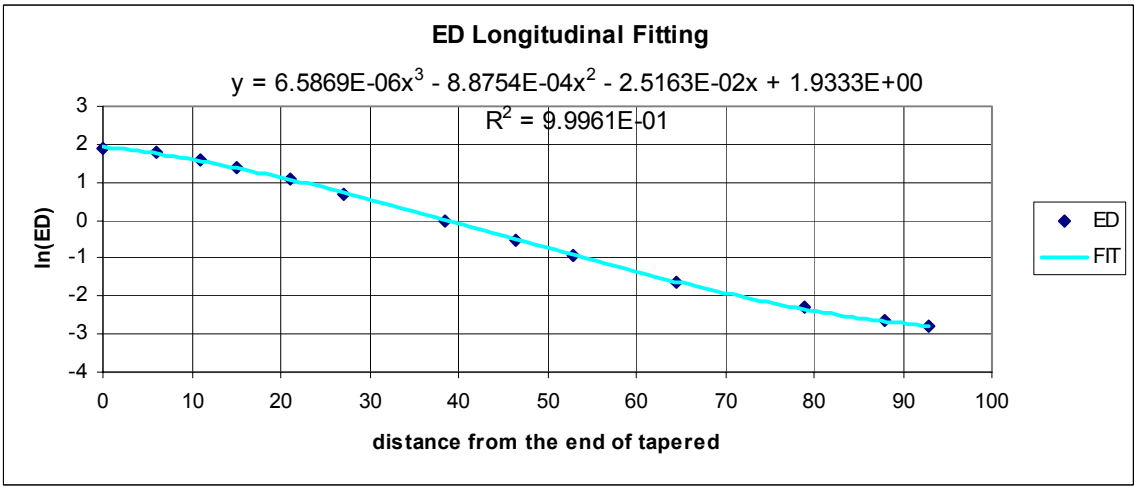

Fig 8 Fitting Longitudinal formula $E_l(z)$

The resulting radial and longitudinal distributions are plotted in Fig.9. The energy deposition is centered at the lower left corner of the stainless vacuum liner.

The factor *F*(*t*) is a function of time. There is from one to ten pulses of beam in each second, and the beam pulse length is 1.6 microseconds. For thermal purposes, the heat deposition in is almost instantaneous. The temperature increase after a single beam pulse is small (for example, 656 joule heat deposition per beam pulse results in temperature increase of less than 0.01°C). Therefore, in this analysis we consider the beam energy deposition as a smoothed function of time. We consider only simplified cases, in which it is either a constant, or a step function.

As a constant, *F(t)* = 8.948e-3 watt/cm^3, calibrated so that the total heating power is 640 watts at level of 1% of the total beam power. For transient analyses, the energy before and after the beam pulse were calculated; the difference is 656 joules. Therefore we just use 656 w for ~1% of the total beam power.

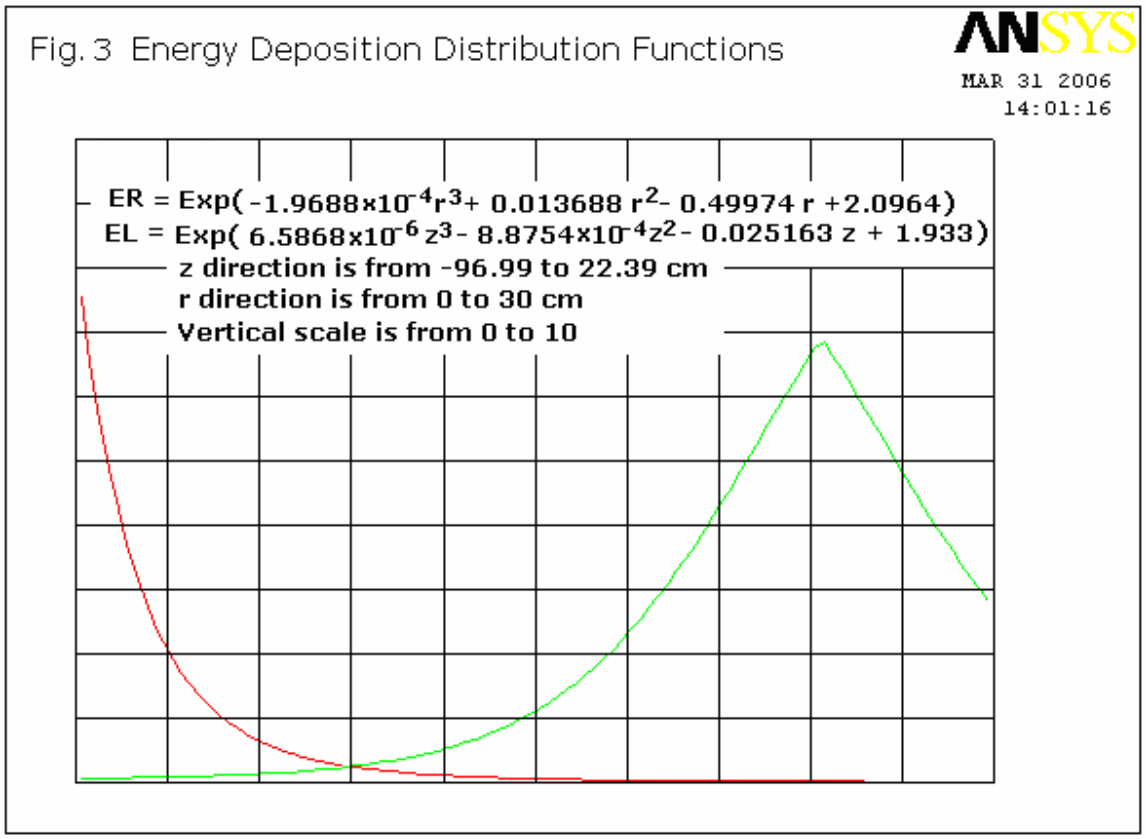

Figure 9 Radial (red) and Longitudinal (cyan) energy deposition functions. Note that longitudinal function is with respect to the absolute distance to the peak.

ANSYS Model

A finite element model is built within ANSYS. The element type is 3D thermal solid Solid70. Fig.10 shows some key points which define the model, and the positions where thermocouples are embedded (the length unit is cm). Fig.11 shows the mesh (for clarity, only a quarter of the model is shown).

In this model, the ambient temperature is set to 25°C. The convection film coefficient is 5 w/m^2-K for side and top surfaces, and 2.5 w/m^2-K for bottom surface. Material properties are as follows. For Stainless Steel, k = 0.162 w/cm-K, ρ = 7.87 g/cm^3, c = 0.5 J/g-K, for carbon steel k = 0.519 w/cm-K, ρ = 7.87 g/cm^3, c = 0.486 J/g-K, and for marble k = 0.03 w/cm-K, ρ = 2.7 g/cm^3, c = 0.88 J/g-K. As for air gap, it is modeled explicitly using contact elements (Conta173 and Targe179). The contact conductance will be thermal conductivity divided by the air gap thickness. At room temperature for 0.1 mm air gap it is 0.03 w/cm^2-K. Considering the elevated temperature and radiation effects, we will use 0.05 w/cm^2-K. Contact elements are added only to the interfaces between different materials. There is no contact thermal resistance between different blocks of the same material in the model. No radiation from external surfaces is considered initially (see below).

In what follows, please use figure numbers from the captions. Labels in the figures are from an earlier report using labels directly from ANSYS.

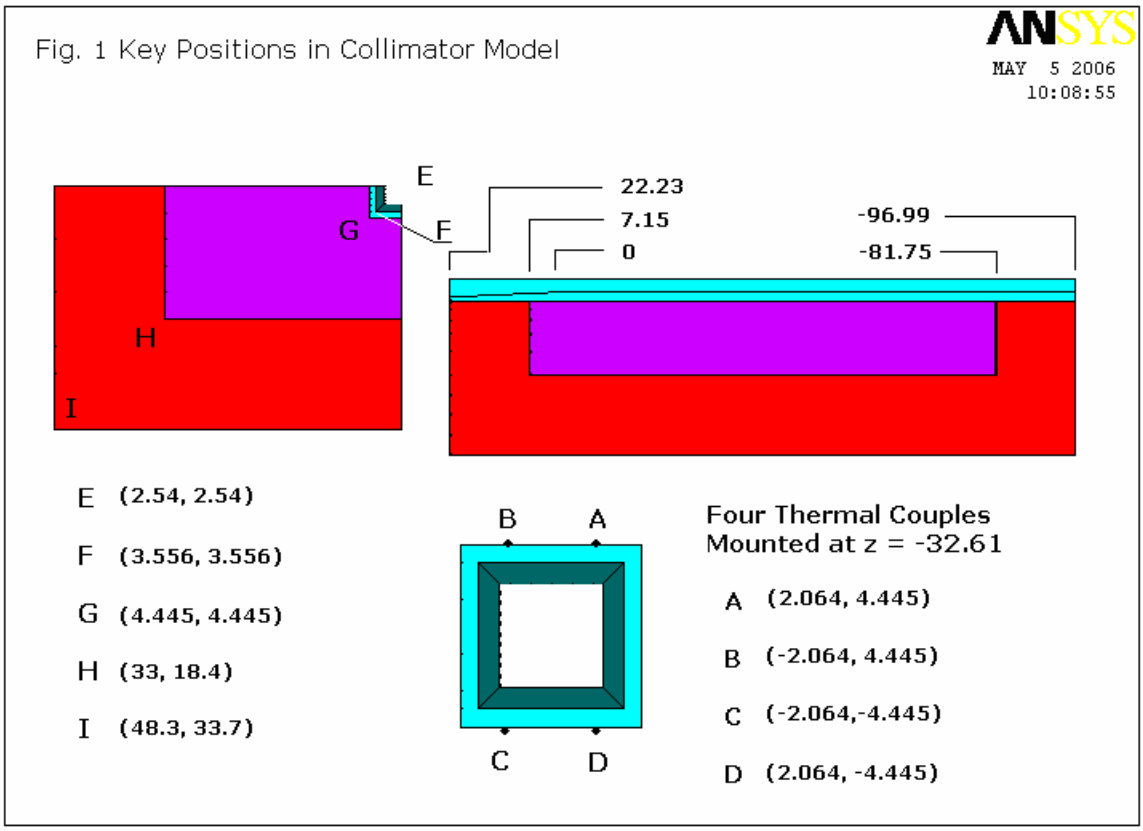

Figure 10 Key positions

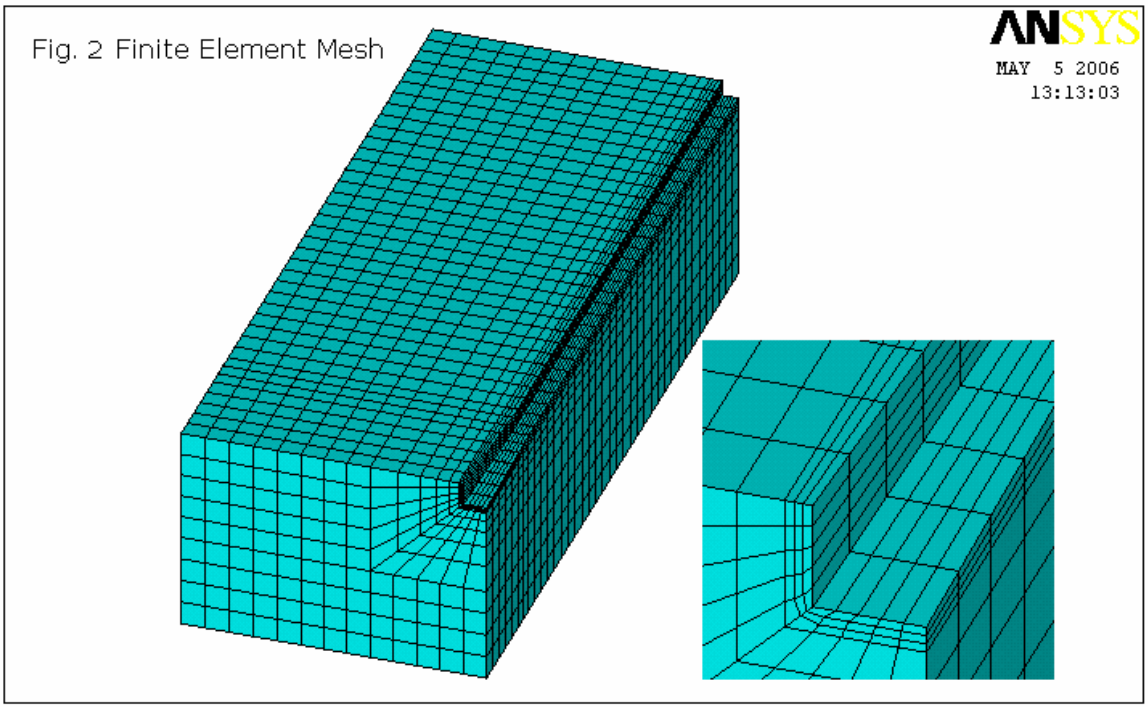

Figure 11 Finite Element Mesh

Static Results

These results describe simulations when the temperature has reached equilibrium; it does not change with time as long as heat load does not change.

Figure 12 (Static Solution) is a typical temperature distribution (for heat load of 656 w). It shows the surface temperature, temperature at $x = 0$, and at $y = 0$, and where the maximum temperature is. The maximum temperature occurs at the lower left corner of the stainless steel near z = 16 cm. (we will call it point M thereafter). This point is upstream of the point of peak power deposition, where the marble (rather than steel) contacts the stainless steel.

Figure 13 (Temperature vs. Load) plots temperatures at points where thermocouples are and the temperature at point M (maximum temperature) with different heat loads. It can be seen that temperatures are linear functions of heat load. For example from the figure, we can get an approximation for maximum temperature as

$$T_M = 25 + 0.234P,$$

$$T_X = 25 + 0.130P.$$

Where head load P is in unit of watt, and temperatures will be in the unit of degree C. T_x is the temperature for any of the thermocouples. In detail, the coefficients for thermocouples A, B, C, and D are 0.127, 0.128, 0.134 and 0.131.

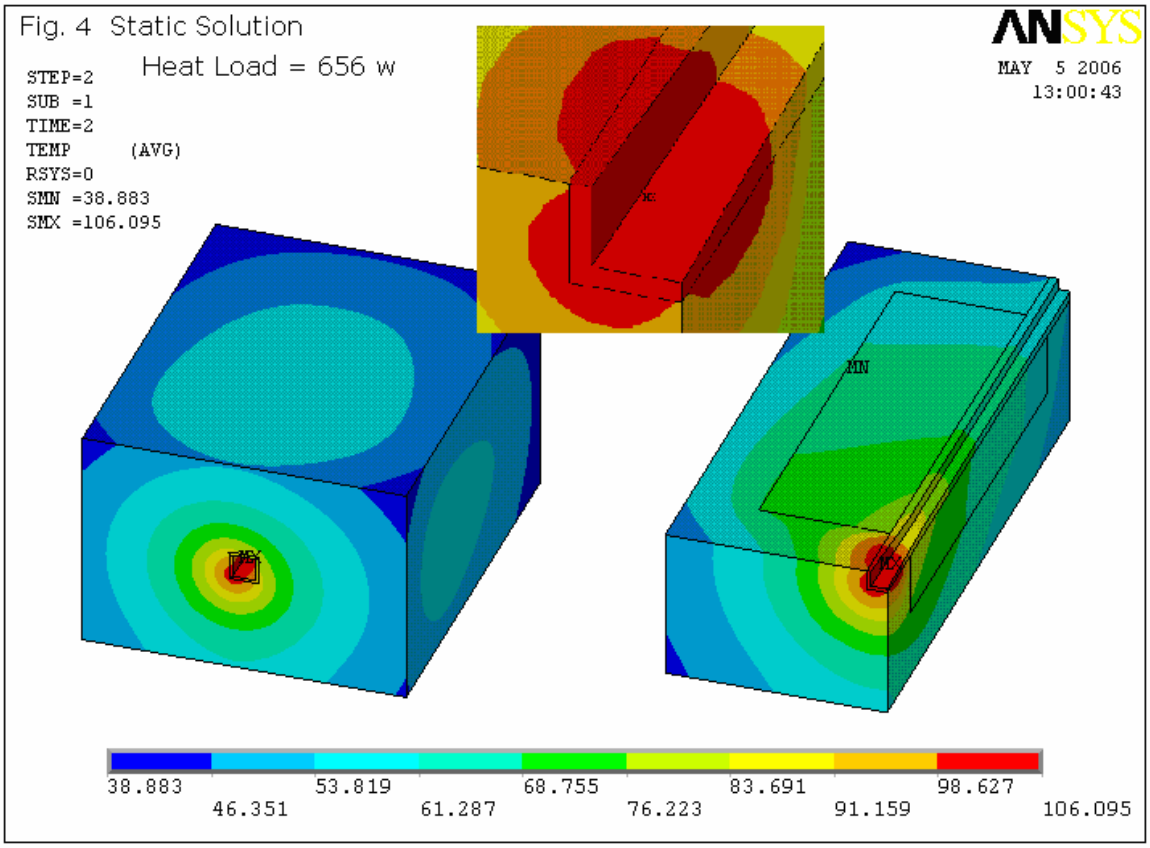

Figure 12 Static Solution

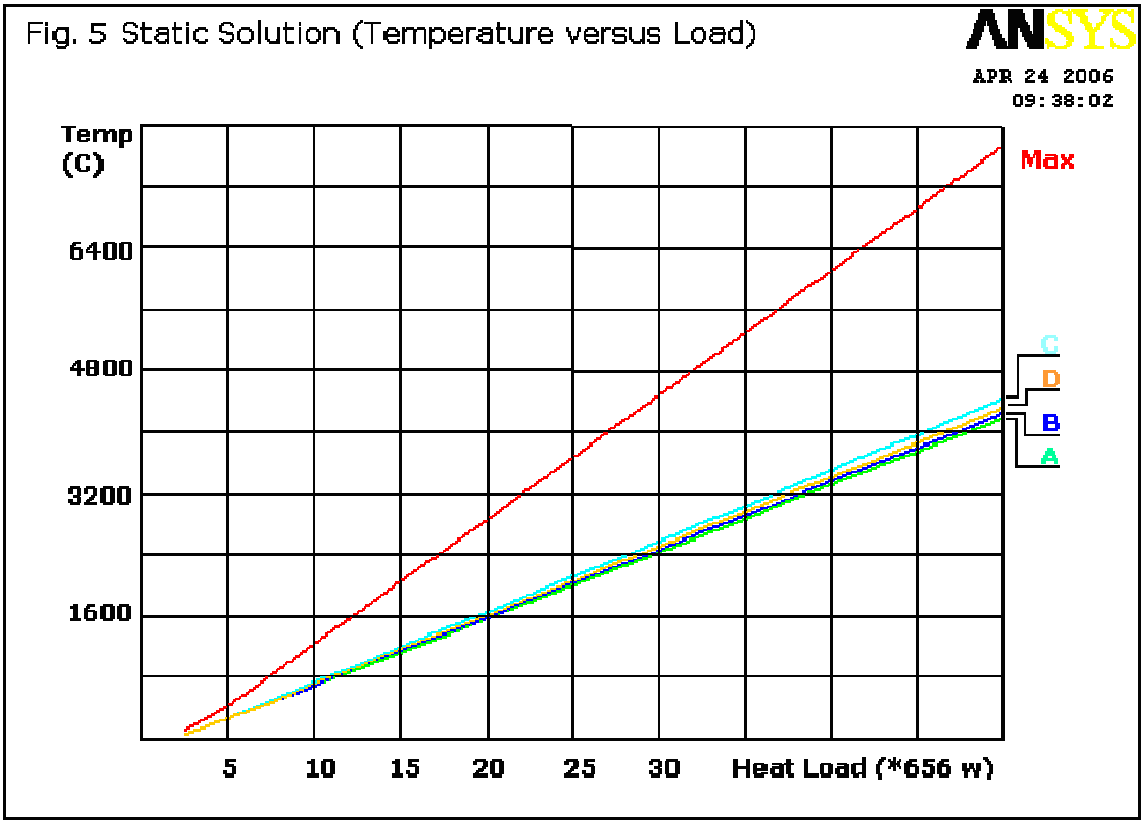

Figure 13 Temperature versus Load

Dynamic Results

Some transient analyses have been done. These results are plotted below.

Fig. 14 is transient temperature for heat load jump from 0 to 656 w, Fig. 15 is from 0 to 6560 w and Fig. 16 is from 0 to 65600 w. A sudden change of beam loss from a stable level was also analyzed. Assuming the stable level is 656W (about 1% of total beam power), Fig. 17 plotted transient response for heat load suddenly changed from 656 w to 10*656 w, Fig. 18 is from 656 w to 20* 656 w, Fig. 19 if from 656 w to 40*656 w.

It can be noted that all the plots of temperature have the similar shape, which can be scaled. Further more, the initial temperature curve after a step change in heat power is quite linear. So we suspect that the initial slope of the temperature curve can be related to the heat power change. Table I shows that this is true. In the table we list results for these as well as additional cases.

Hence we can relate the temperature measurement to the beam heating power. If the measured temperature is constant, we know what the heating power is from the static solution. And if the measured temperature begins to increase or decrease, from the rate of change we know the heat power change. The initial rate-of-rise of temperature change per 10 seconds per 100*656 w is 1.13 (A), 1.77 (B), 11.95 (C) and 3.56 (D). Or we can write it as

$$\frac{dT/dt}{\Delta P} = 1.72\times10^{-6}, 2.70\times10^{-6}, 1.82\times10^{-5}, 5.43\times10^{-6}\ C°/J.$$

It tells us that it takes a large amount of beam loss to heat up the collimator significantly.

If we use the rate-of-rise temperature measurement as the indication of beam loss, then we write:

$$\frac{\Delta P}{dT/dt} = 5.81\times10^5, 3.70\times10^5, 5.49\times10^4, 1.84\times10^5 \; Watt/(C^\circ/s).$$

For example, at tempC, a rate-of-rise of 1 C^o/s will indicate the power loss increased of 54.9kW, 1 C^o/min for an increase of 915 Watts. tempC is most sensitive one among the four, but it may still not good enough for beam loss less than 0.5% (320Watts).

Case	dPower	dTempA	DTempA	dTempB	DTempB	dTempC	DTempC	dTempD	DTempD
c65600	100	1.1274	1.1274	1.7664	1.7664	11.947	11.947	3.5629	3.5629
c06560	10	0.1127	1.127	0.1766	1.766	1.1947	11.947	0.3563	3.563
c00656	1	0.0113	1.13	0.0177	1.77	0.1195	11.95	0.0356	3.56
c01-40	39	0.4399	1.128	0.689	1.767	4.6596	11.948	1.3901	3.564
c01-20	19	0.2144	1.128	0.3358	1.767	2.2702	11.948	0.6776	3.566
c01-10	9	0.1017	1.13	0.1591	1.768	1.0754	11.949	0.3213	3.57
c01-05	4	0.0453	1.133	0.0708	1.77	0.4781	11.953	0.1431	3.578
c02-10	8	0.091	1.137	0.142	1.775	0.956	11.95	0.286	3.575
c02-20	18	0.204	1.133	0.319	1.772	2.151	11.95	0.643	3.572
c02-40	38	0.429	1.13	0.672	1.768	4.54	11.947	1.355	3.566
c05-10	5	0.057	1.14	0.09	1.8	0.598	11.96	0.181	3.62
c05-20	15	0.17	1.133	0.266	1.773	1.793	11.953	0.537	3.58
c05-40	35	0.396	1.131	0.62	1.771	4.138	11.823	1.25	3.571

Table I

Temperature differentials and normalized differentials after 10 seconds at new heating power.

In this table, case c00656 is the transient response of collimator subjected to 656 w heating power with initial condition of uniform 25 degree C. So case c06560 is the case of 6560 w heat power, case c65600 is the case with 65600 w heating. The case c01-40 is the solution of 40*656 w heating, with initial condition of static solution of 1*656 w. And so on. dPower is the heating power change in the case (measure in the unit of 656 w). dTempA is the temperature increase per 10 seconds measured at thermal couple A after the heat power have a step change. DTempA is the slope data normalized with 100*656 w heat change.

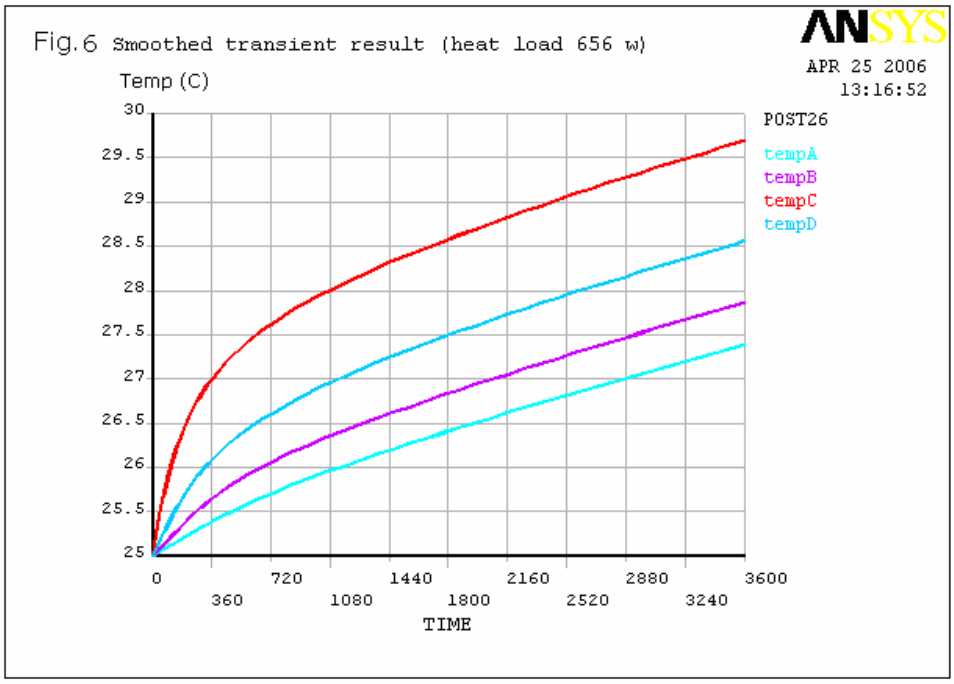

Figure 14 Transient for 0 to 656 w

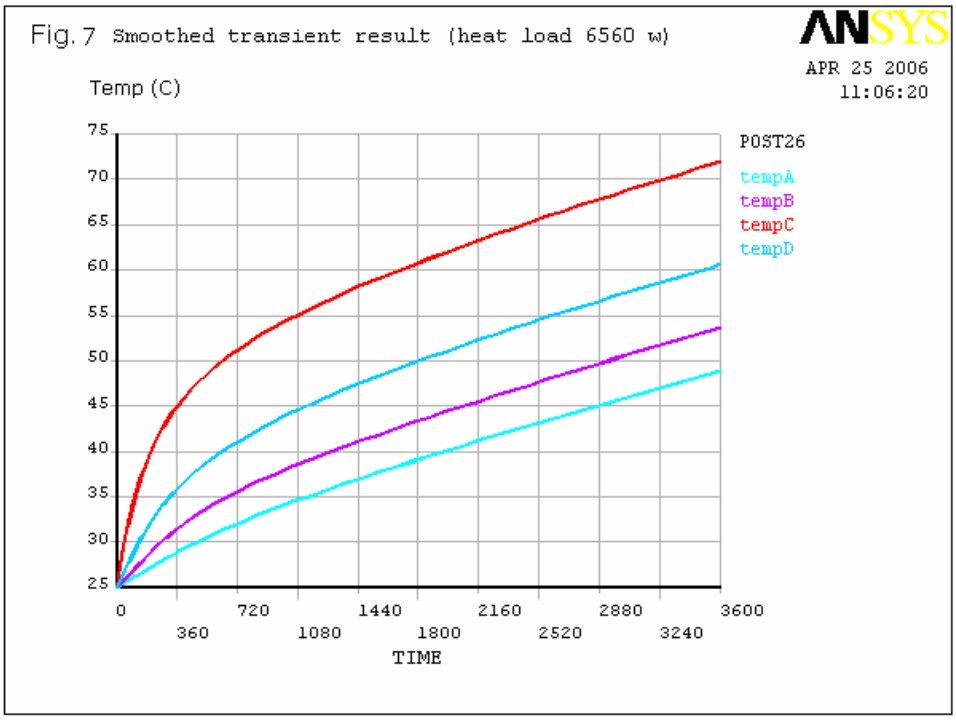

Figure 15 Transient from 0 to 6560 w

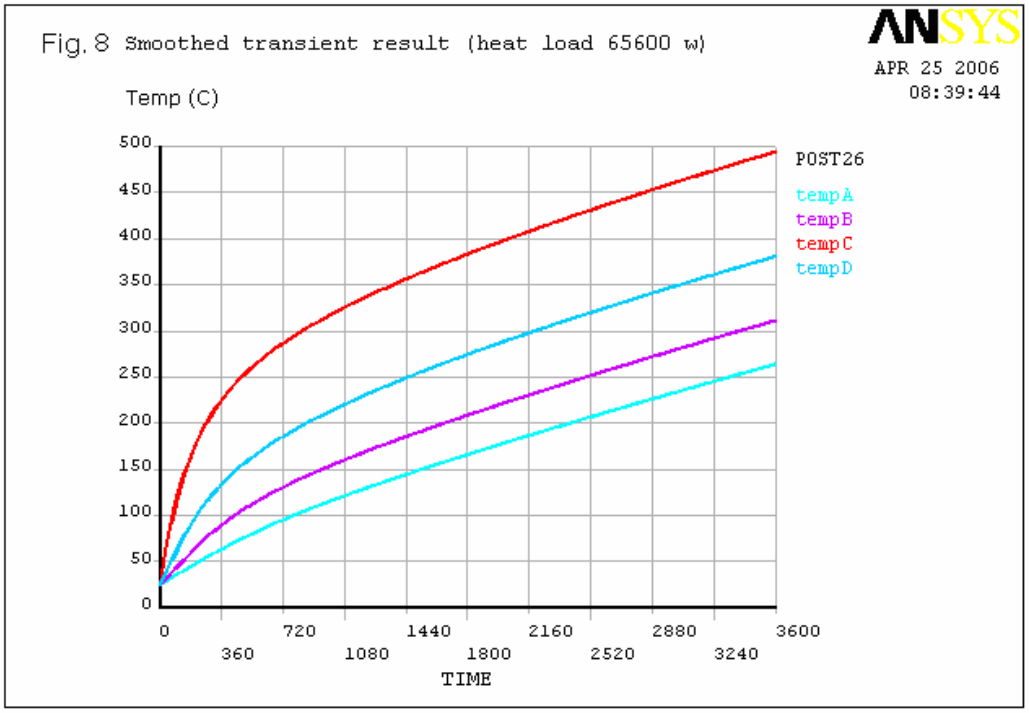

Figure 16 Transient from 0 to 65600 w

The results in Table I describe the initial temperature changes in the first seconds after a change in lost beam power. We note that the initial rise is about 10 times faster for thermocouple tempC than it is for tempA (the furthest from the peak input power). This fast rise is associated with the thermal capacity of the stainless steel vacuum liner. After about 720 sec (12 minutes), the rise becomes linear with a very much lower slope. For input power from 1 * 656 w to about 10 * 656 w, tempC rises about 1 x 10^{-6} ^{o}C /J with tempA at about 80% of that slope. For beam power input of 20 to 40 times 656 w, the thermocouples show a slope which is 2 to 4 times higher in the period from 720 sec (12 minutes) to 3600 sec (60 minutes).

Figure 23 (Figure 24) shows the temperature profile for 0 w input after equilibrium at 656 w (6560 w) input. We see that the four thermocouples which were at ~70^{o} C drop about 4 degrees in 3600 seconds while for initial temperature of about 460^{o} C the drop is about 20 degrees. This gives similar rate of change when the input rate has a negative change as for a positive change (to an accuracy of 30% or so) so we can assume that there are no huge non-linearities in using the integral of the temperatures to measure the integral beam power deposited. Beam heating power of more than a few percent will not be permitted and interlocks on loss monitors as well as interlocks on the thermocouples will prevent that occurrence. For that reason, the modest non-linearities associated with higher beam loss power will not happen and the integration of temperature vs. time should be linearly related to the integrated beam loss.

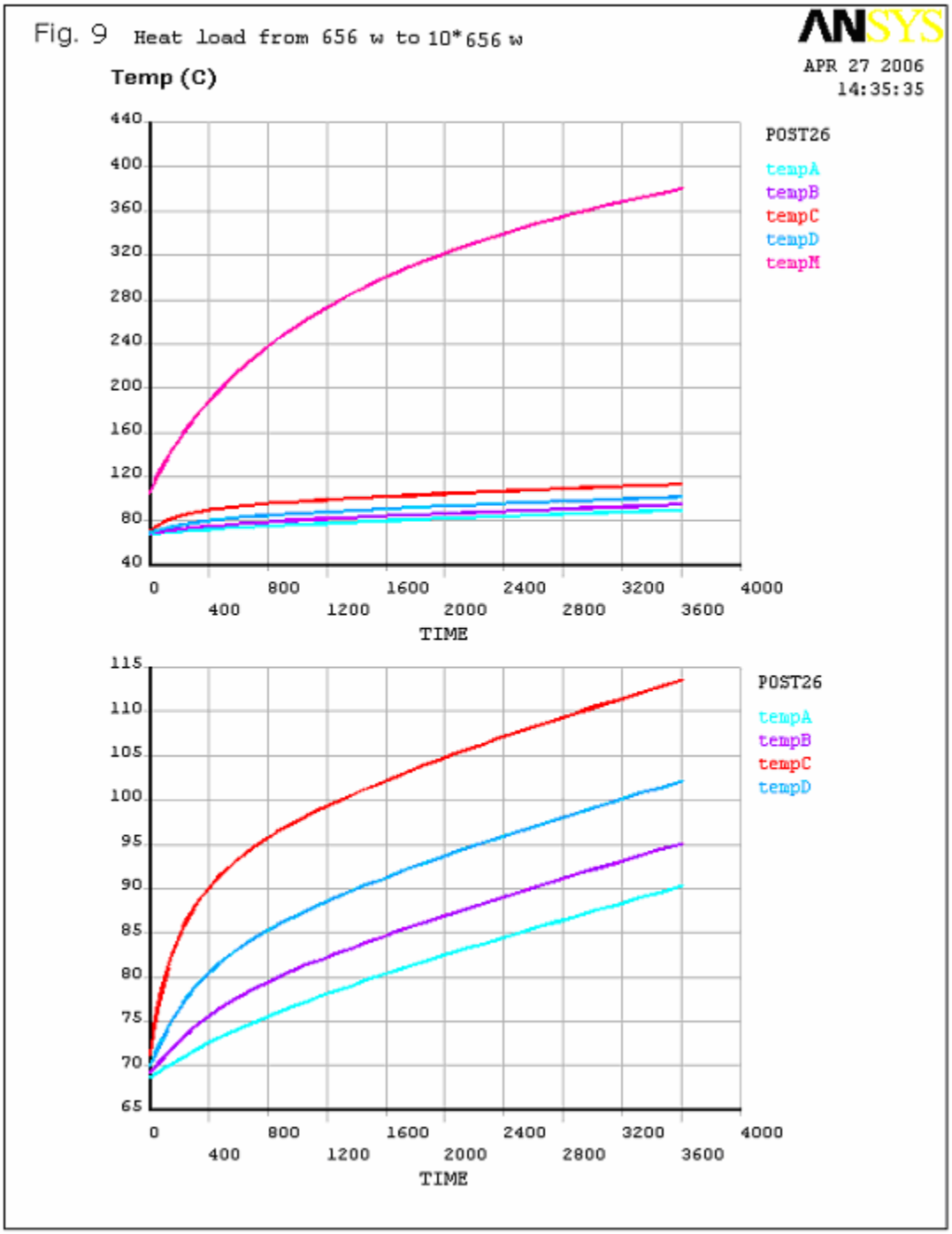

Figure 17 Transient from 656 w to 10 * 656 w

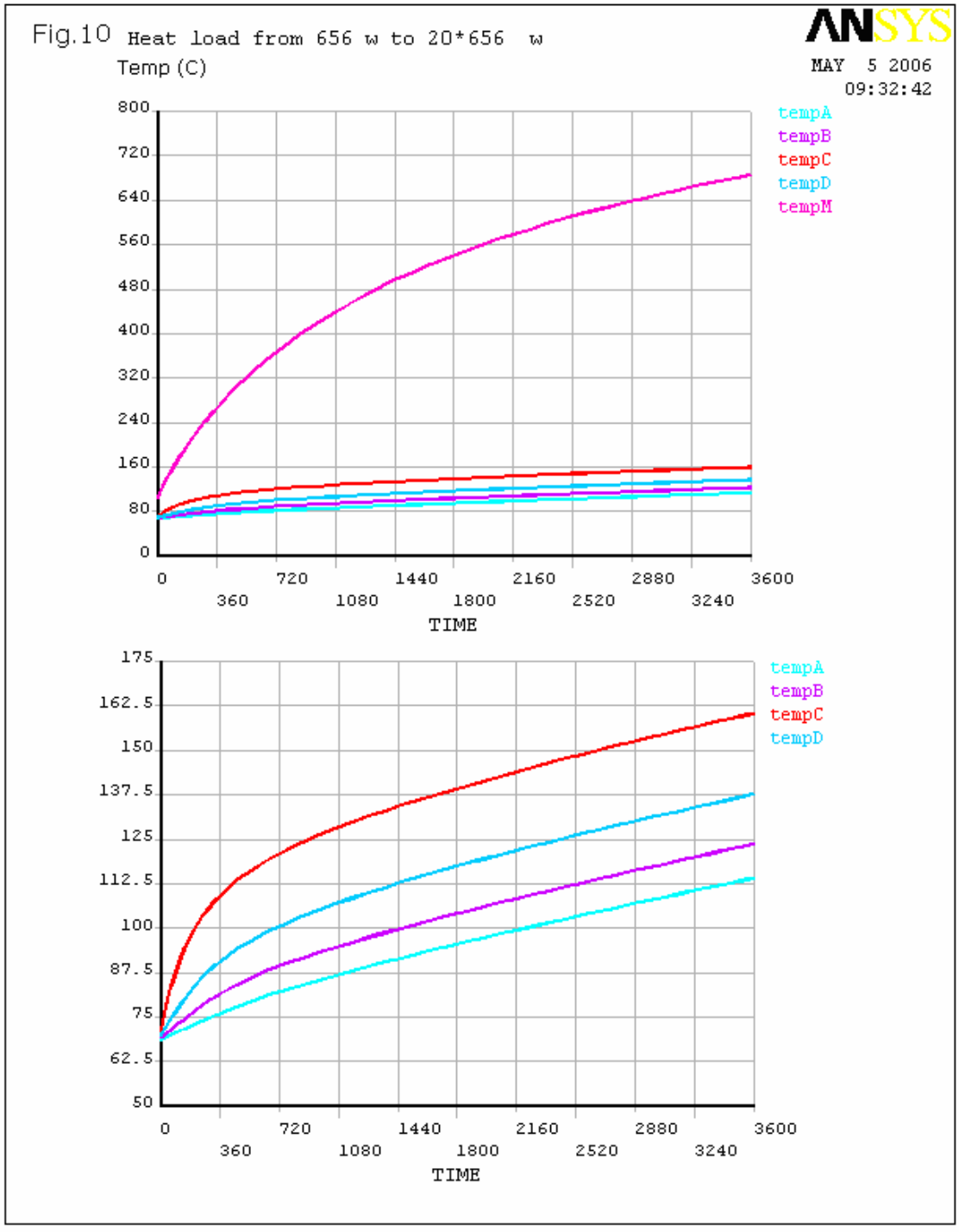

Figure 18 Transient from 656 w to 20 * 656 w

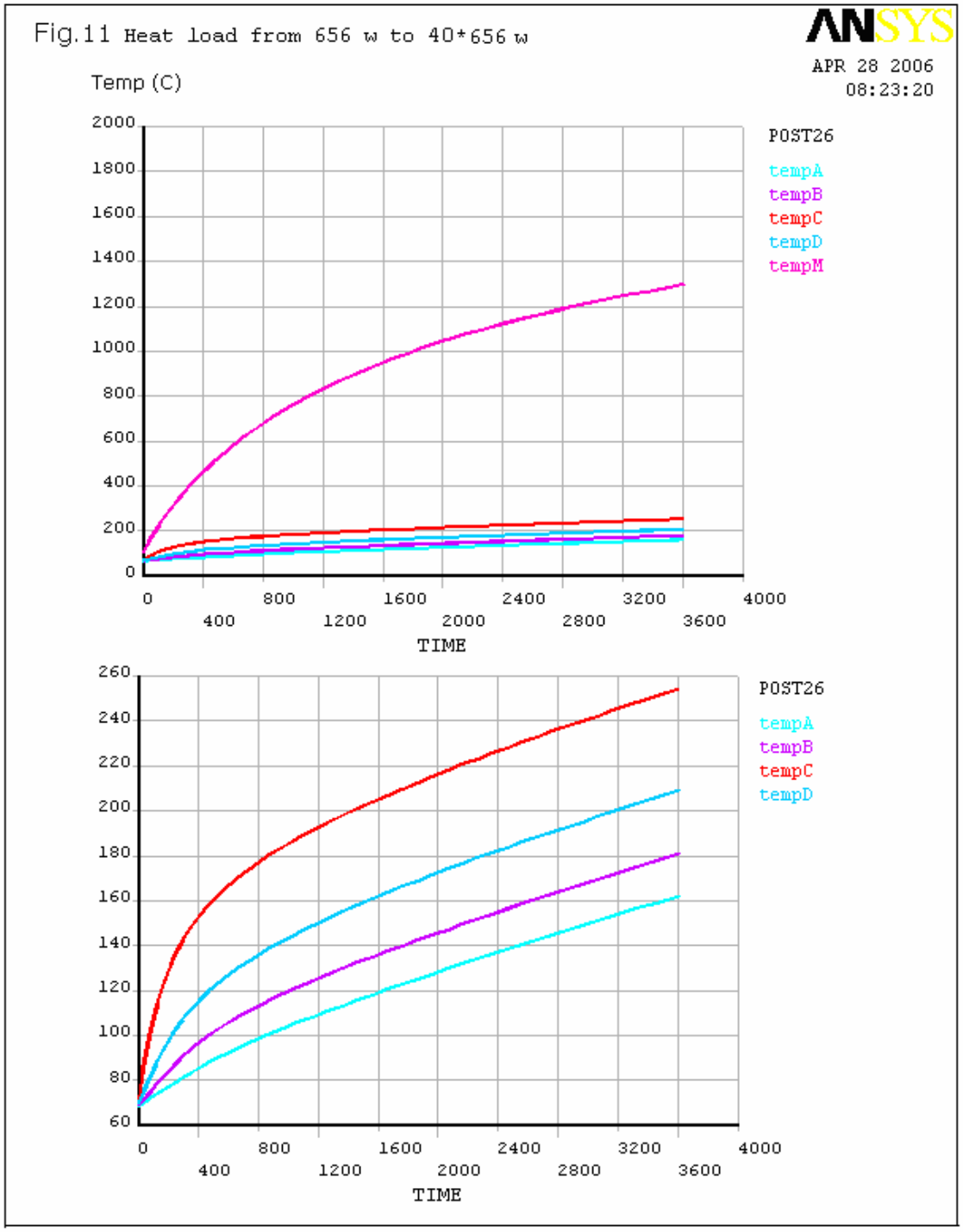

Figure 19 Transient from 656 w to 40 * 656 w

Calibration

We expect to compare these calculations with temperature measurements taken with known beam power deposited in the collimators. Reliable beam loss measurements are available from the beam toroids if we lose a large fraction (30% to 100%) of the beam. We will only be

able to do transient heating measurements -- never reaching equilibrium -- with a beam loss measured by toroids. We may be able to span the gap by calibrating the loss monitors at low intensity, establishing the thermocouple response there and moving up to higher intensity but modest loss and calibrate the thermal response, holding the pulse-by-pulse loss constant and upping the repetition rate.

Uncertainties

There are some uncertainties about our finite element model.

First, the material properties are assumed to be constants. In fact, they should be functions of temperature. For example, stainless steel has thermal conductivity of 16.2 w/m-C at 100^{o}C, and 21.5 w/m-C at 500^{o}C. This larger thermal conductivity at high temperature means we have less thermal gradient, and hence the maximum temperature would be smaller.

Second, the contact thermal resistance is a pure estimation, not a measurement. If this number is changed, we expect our results will change too. What happens if the resistance is twice as large as our estimated value? To see the sensitivity of our result to this number, we did a comparison which is shown in Fig. 20. From the figure, we see that the influence of the contact thermal resistance is not very significant.

Third, the boundary condition is uncertain. In the model we assume the convection coefficient of 5 W/m^2-C at top and sides, and 2.5 W/m^2-C at bottom. However, it will increase as the surface temperature or/and ambient temperature rise. Radiation effects are neglected. As the surface temperature increases, the radiation effect will be more and more important, as shown in Fig. 21. Including radiation effects will reduce the surface temperature, as well as the maximum temperature. Fig. 22 shows the comparison of static temperature with and without radiation. We see that, with radiation, temperature becomes lower, and the relation between temperature and heat load is no longer linear.

In case of mis-steering beam or misalignment of collimators, the beam energy deposited in collimator can differ significantly from the results in MARS simulation. Therefore the temperature distribution will be different from this ANSYS results. However, the beam position monitoring combined with beam optics constraints makes it unlikely that the beam will strike the collimator in a very different place.

The 5th thermal couple at upstream of the vacuum tube will be heated to 80-100C^{o} with 1% beam loss, about the same scale as the embedded ones. Certainly it will be helpful for determining if the heating spot moves longitudinally.

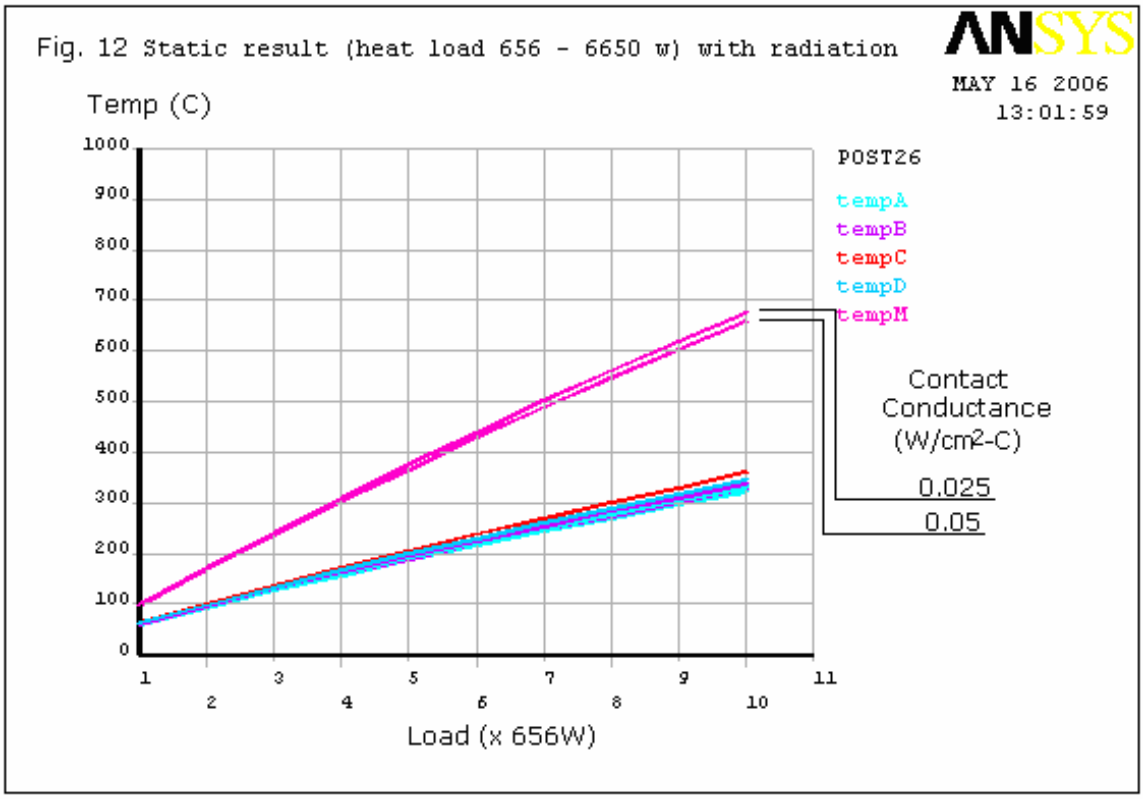

Figure 20 Static response with different contact conductance

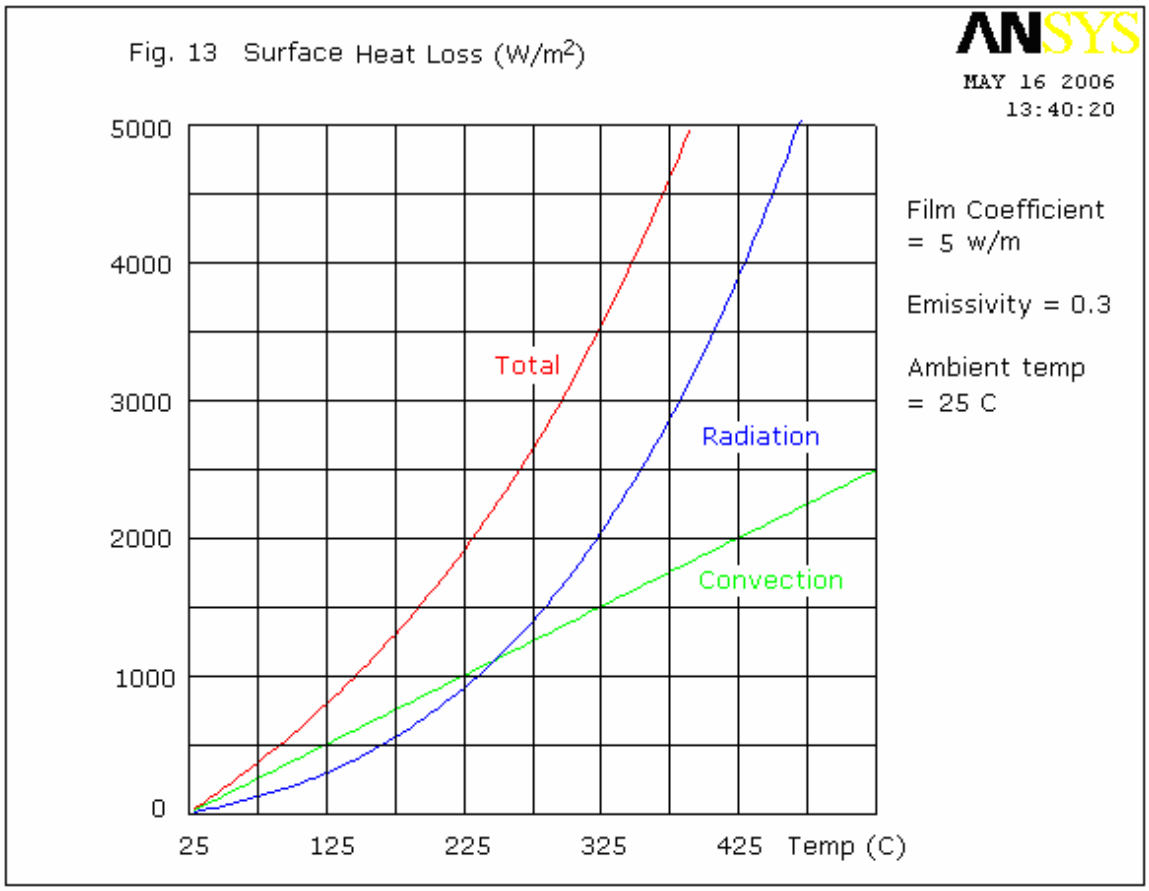

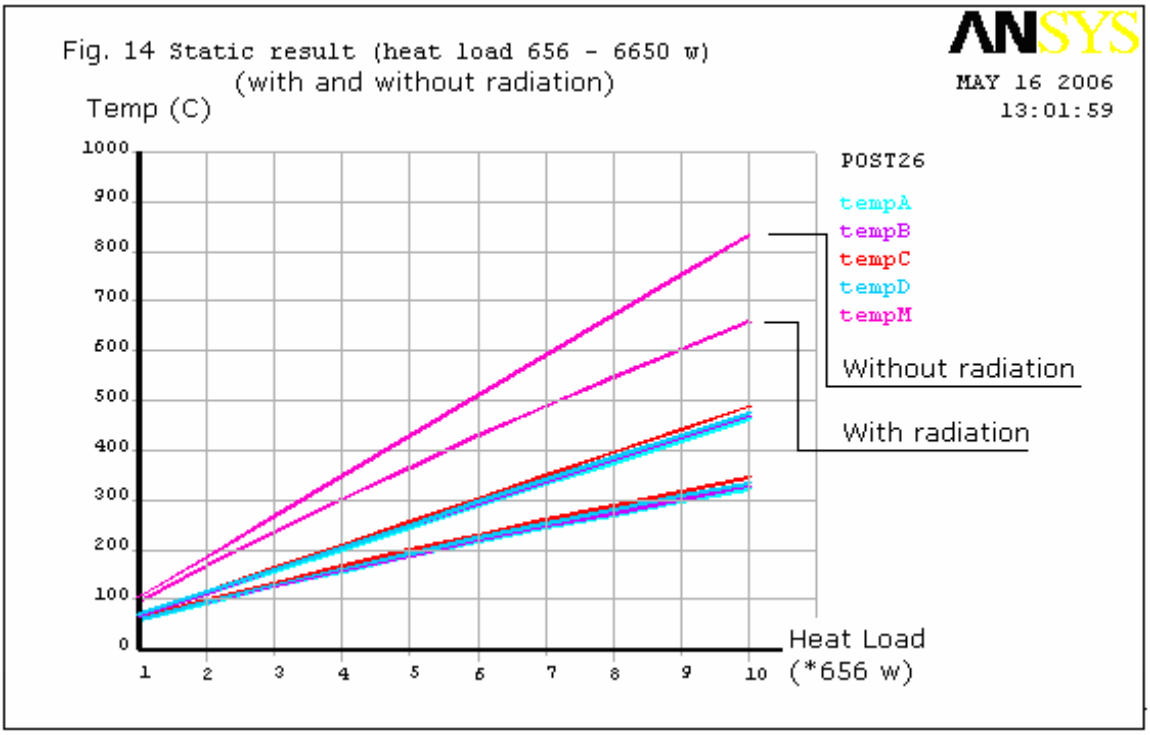

Figure 21 Surface Heat Loss Figure 22 Static simulation with/without radiation

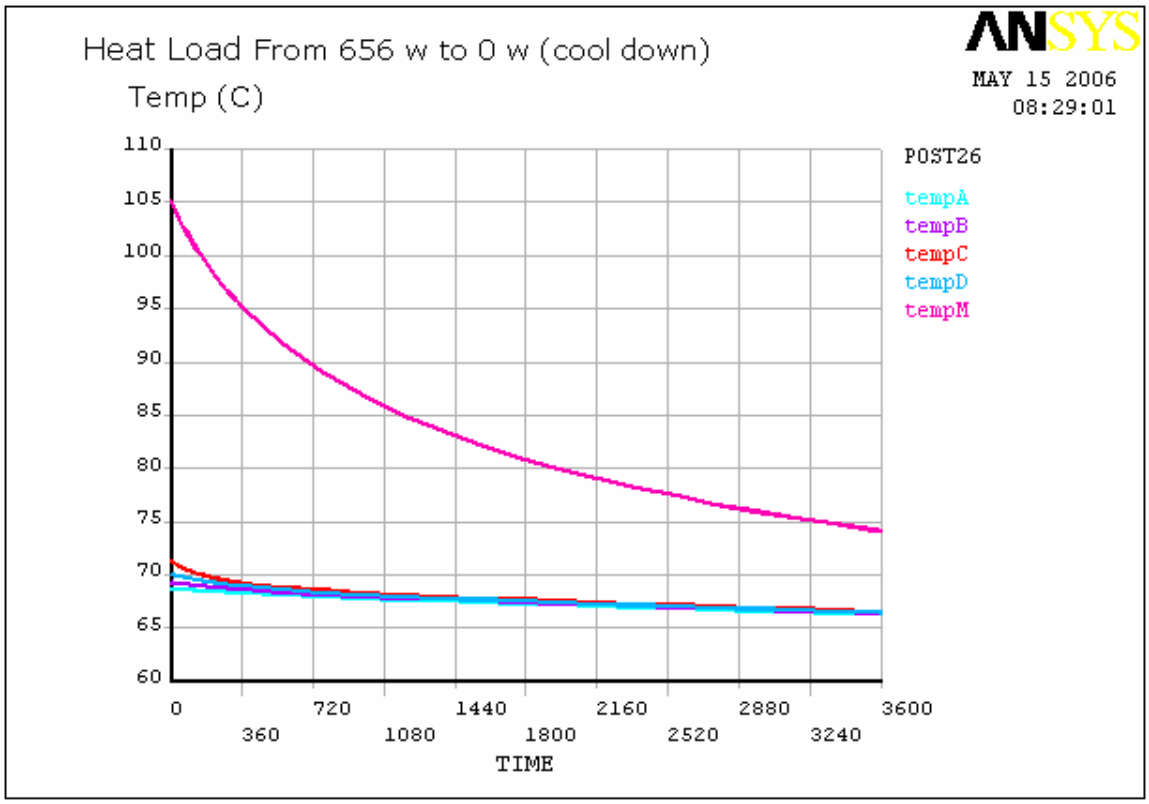

Figure 23 Cooling curve from 656 w equilibrium with 0 w input

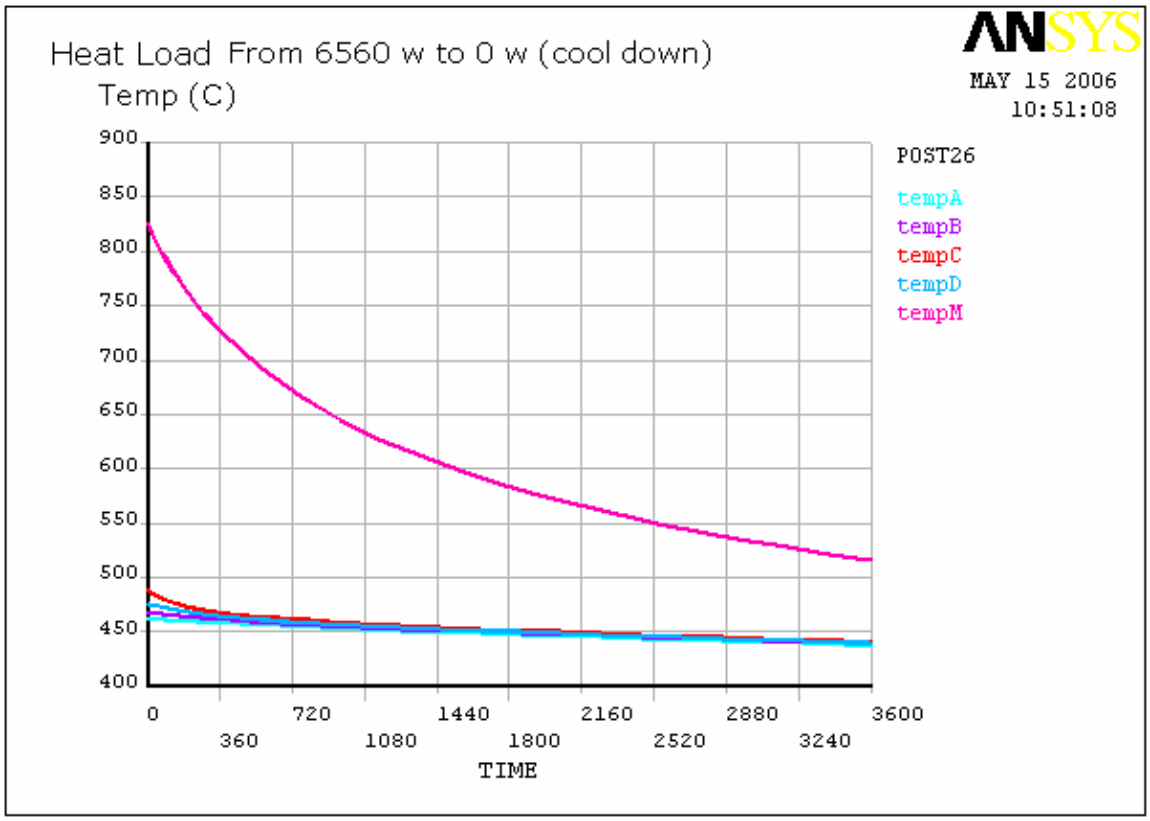

Figure 24 Cooling curve from 6560 w equilibrium with 0 w input

Conclusions

Thermal analysis of collimator operation was carried out in both static and transient simulations. Both normal operation and accident cases were simulated. Local temperature at thermal couples was predicted in different operation cases. Uncertainties associated with this analysis were discussed. The additional (upstream) thermocouple should be helpful. Thermocouples should be adequate for device protection. Trips based on thermocouple temperature readings should provide adequate protection even in case of deposition of the full beam into one collimator. Integration of the thermocouple temperatures should provide a measure of the total radiation.

References

[1] N.V. Mokhov, et al., "Fermilab booster beam collimation and shielding", FERMILAB-CONF-03-087, May 2003. 4pp.
Presented at Particle Accelerator Conference (PAC 03), Portland, Oregon, 12-16 May 2003.

[2] Vladimir Sidorov, Al Legan and Bruce C. Brown, "Mechanical Design of MI8 Collimators", Beams-doc-2287.

[3] Nikolai Mokhov and Bruce C. Brown, "MARS Calculations for MI8 Collimator Design", Beams-doc, to be submitted.

[4] ANSYS Operations Guide, Release 10.0, 2005, ANSYS, Inc.

[5] ANSYS Analysis Guide, Release 10.0, 2005, ANSYS, Inc.